Tuning exciton complexes in twisted bilayer WSe_2 at intermediate misorientation

Rahul Debnath,[1,*] Shaili Sett,[1] Sudipta Kundu,[1] Rabindra Biswas,[2] Varun Raghunathan,[2] Manish Jain,[1] Arindam Ghosh,[1,3] and Akshay Singh[1]

[1]*Department of Physics, Indian Institute of Science, Bangalore 560012, India*

[2]*Department of Electrical and Communication Engineering, Indian Institute of Science, Bangalore 560012, India*

[3]*Centre for Nano Science and Engineering, Indian Institute of Science, Bangalore 560012, India*

(Received 31 March 2022; revised 22 August 2022; accepted 30 August 2022; published 9 September 2022)

Twist angle modifies the band alignment, screening, and interlayer (IL) coupling in twisted bilayers (tBLs) of transition metal dichalcogenides. Intermediate misorientation (twist angles $> 15^\circ$) bilayers (BLs) offer a unique opportunity to tune excitonic behavior within these concurrent physical mechanisms but are seldom studied. In this paper, we measure many-body excitonic complexes in monolayer (ML), natural BL, and tBL WSe_2. Neutral biexciton (XX) is observed in tBL, while being undetected in nonencapsulated ML and BL, demonstrating unique effects of disorder screening in tBLs. The XX as well as charged biexciton (XX^-) are robust to thermal dissociation and are controllable by electrostatic doping. Vanishing of momentum-indirect IL excitons with increasing electron doping is demonstrated in tBL, resulting from near alignment of Q'-K and K-K valleys. Intermediate misorientation samples offer a high degree of control of excitonic complexes while offering possibilities of studying exciton-phonon coupling, band alignment, and screening.

DOI: 10.1103/PhysRevB.106.125409

I. INTRODUCTION

A moiré potential results from the relative atomic arrangement when two van der Waals materials are stacked together at zero or relative twist angles. Twisted bilayers (tBLs) of two-dimensional (2D) transition metal dichalcogenides (TMDCs) exhibit opto-electronic features as a result of the underlying emergent potential [1,2]. The rotational alignment between the two layers has emerged as a key degree of freedom that can control the momentum alignment of the valleys and the hybridization of respective layers [3,4]. Emergent phenomena such as interlayer (IL) excitons localized by the moiré potential [5,6], observation of hybridized excitons [7,8], and antibunching of moiré exciton emission [9] have been established. Many-body correlated physics, ranging from moiré excitons and moiré trions [10], the Stark effect in excitons [11], the Wigner crystal state [12], and stripe phases [13] have been observed in tBLs of TMDCs.

WSe_2 in the 2D limit (with large spin-orbit coupling) is ideal for hosting multiparticle bound states due to reduced dielectric screening of Coulomb interactions, resulting in formation of tightly bound excitons and correlated excitonic states [14]. The WSe_2 bandgap changes from a direct K-K transition (in the monolayer) to an indirect gap Q-K transition in the bilayer (BL) [15]. The relative band alignment of Q' and K valleys is also sensitive to the rotational alignment between the layers [16–18], making WSe_2 an ideal platform for studying the momentum-indirect spectral emissions. Authors of studies on excitons in WSe_2 and other TMDCs have primarily focused on identification of multiparticle bound states in MLs and natural BLs [19–22]. Established spectral features include bright neutral exciton (X^0) and trions (X^-, X^+) and a dark exciton (X^D). The dark exciton [22–24] has an out-of-plane dipole and usually cannot be spectroscopically observed unless using a large numerical aperture (NA) objective or in-plane magnetic field [25–27]. A schematic of the formation of bright and dark excitons is shown in Fig. 1(a). Exhaustive investigations involving electrostatic doping, power-dependent photoluminescence (PL), and thermal activation studies have established that emission features at 18–25 meV and 47–54 meV below X^0 are the biexciton (XX) and charged biexciton (XX^-), respectively [25,28–30]. Figure 1(b) shows a schematic of the formation of these higher exciton complexes. At higher electron doping, a doubly negative charged trion (X^{--}) has also been observed [31]. Understanding the physical behavior of multiparticle states with temperature and electrostatic doping is essential to harness the true capability of the twisted artificial systems in opto-electronic applications and is the main focus of this paper.

In this paper, we combine PL spectroscopy over a broad temperature range and first-principles density functional theory (DFT) analysis to study the interplay of charge, layer coupling, and band structure in $\approx 20^\circ$ tBL WSe_2 as well as its ML and BL counterparts. We observe higher-order excitonic complexes at high temperatures in all the WSe_2 samples, with majority PL contribution in the high electron-doped regime. Our measurements demonstrate the spectral signature of the neutral biexciton in tBL WSe_2 up to 180 K, signifying its robustness and stability, and effects of screening. Thermally activated measurements were performed to explore the

*rahuldebnath@iisc.ac.in

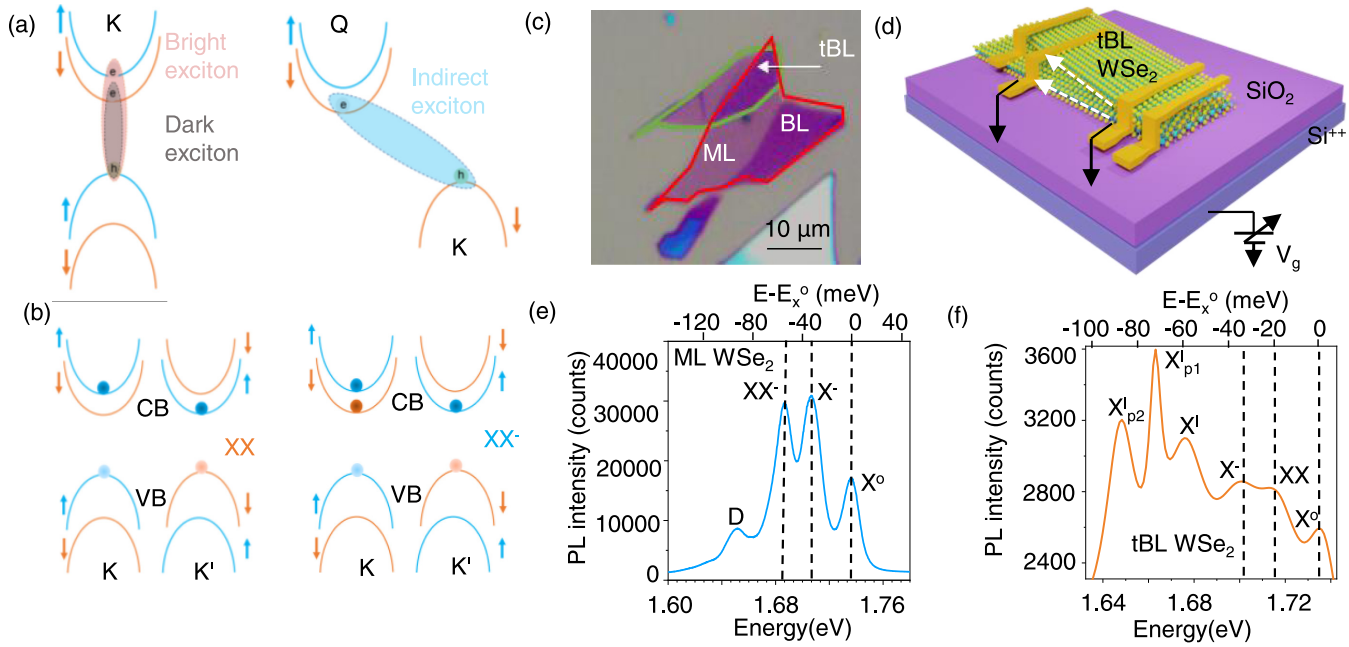

FIG. 1. Bound exciton states, device configuration, and photoluminescence (PL) spectra in WSe_2. (a) and (b) Schematic of multiparticle bound states in monolayer (ML) and bilayer (BL) WSe_2. The K and K' valleys are shown in different colors. The arrows signify the spin of the charged particle. The electrons are shown as opaque circles, while the holes are transparent circles. The schematic shows the bound states of the neutral exciton (X^0), dark exciton (X^D), indirect interlayer exciton (X^I), neutral biexciton (XX), and negatively charged biexciton (XX^-). (c) Optical image of WSe_2 with ML, BL, and twisted bilayer (tBL) regions. (d) Device schematic with electrical configuration. (e) and (f) PL spectra of ML and tBL WSe_2 at temperature 7 K. X^D, XX^-, negatively charged trion (X^-), X^0, XX, X^I, and phonon replicas (X^I_{p1}, X^I_{p2}) are indicated.

underlying energetics of the exciton complexes, using which we determined their binding energy (BE) and established their presence in the WSe_2 system. Additionally, power-dependent PL for XX shows super-linear power dependence, further supporting the peak assignment of XX. Further, the twist angle causes a shift in the energy of phonon-assisted momentum-indirect IL excitons, and these observations are corroborated by DFT calculations. Remarkably, IL exciton in the tBL shows asymmetric PL spectra with doping, which is attributed to near alignment of Q-K and K-K transitions. Overall, in this paper, we provide insights into the charge tunability of the higher-order excitonic complexes in intermediate misorientation tBL WSe_2.

II. RESULTS AND DISCUSSION

A. Device configuration of tBL WSe_2

Figure 1(c) shows the tBL WSe_2 heterostructure. The transferred 2D stack has three distinct portions: ML, natural BL (marked as BL), and tBL. The relative rotation between the individual layers is $20^\circ \pm 0.5^\circ$, which has been verified optically [32] and by second harmonic generation (SHG). Details are given in Supplemental Material Sec. I [33]. A field-effect transistor structure is fabricated which is equipped with a global SiO_2 back gate for electrostatic doping, and the individual 2D layers can be grounded through the metallic contacts (Cr/Au), as shown in the schematic of Fig. 1(d). PL measurements were performed using a 532 nm continuous-wave laser.

B. Excitonic complexes in a WSe_2 system

The device design enables measurement of PL in three distinct systems under identical temperature and doping conditions. Figures 1(e) and 1(f) show the PL spectrum of ML and tBL WSe_2, respectively, at 7 K. In ML and BL WSe_2 (see Supplemental Material Sec. II [33] for PL data on BL), under zero gate bias, we observe three excitonic species: X^0 at 1.736 eV, X^- (34 meV below X^0), and XX^- at 1.685 eV (17 meV below X^-) [25,31,34]. We note that there is significant peak broadening that disallows differentiation between XX^- and X^{--} peaks at high electron doping, and thus, we denote the peak as $XX^-(X^{--})$. Apart from identification of the excitonic peaks from their spectral position, further evidence is provided by thermal activation studies to determine the BE, as discussed in the last section of this paper. The lower energy peaks from 1.5–1.65 eV in the tBL are attributed to the indirect excitons (X^I), occurring due to the indirect momentum Q'-K transition. The energetic position of the Q' point in the Brillouin zone is discussed in Supplemental Material Sec. V [33]. Multipeak Lorentzian fits to the PL spectra for all devices are given in Supplemental Material Sec. II [33]. Table I provides the peak positions of the various excitons observed in the WSe_2 system and compares them with those available in the literature. It is to be noted that the absolute peak position for excitonic complexes depends on the sample quality and dielectric environment. However, the relative difference in peak position (BE) of the excitonic complexes is unlikely to change between samples. We have observed BE for excitonic complexes in our samples like those in the literature.

TABLE I. Identification of excitonic peaks in the WSe_2 system.

Excitonic peak	Peak position (eV)	
	This paper	Literature
X^0	1.736 (ML), 1.735 (tBL)	1.733 (ML) [35], 1.708 (ML) [25], 1.74 (ML) [20]
X^-	1.702 (ML) $\Delta = 34$ meV	1.697 (ML) $\Delta = 36$ meV [35], 1.673 (ML) $\Delta = 35$ meV [25], 1.705 (ML)
	1.703 (tBL) $\Delta = 32$ meV	$\Delta = 35$ meV [20]
XX	1.715 (tBL) $\Delta = 20$ meV	1.69 (ML) $\Delta = 18$ meV [25], 1.715 (ML) $\Delta = 18$ meV [35], 1.723 (ML) $\Delta = 17$ meV [20]
XX^-	1.685 (ML) $\Delta = 51$ meV	1.684 (ML) $\Delta = 49$ [35], 1.659 (ML) $\Delta = 49$ [25], 1.691 (ML) $\Delta = 49$ [20]
	1.686 (tBL) $\Delta = 49$ meV	
X^I (tBL)	1.675 (20° tBL)	1.59 (21° tBL) [36], 1.607 (17° tBL) 1.525, 1.512 (0° tBL) [36,40], 1.618 (high angle, tBL) [37]
X_p^I (tBL)	1.660, 1.647	1.5–1.7 eV [38]
X^I (BL)	1.57	1.568 [40], 1.569 [37]

C. Electrostatic tuning of many-body states

We now investigate the gate-voltage dependence of the PL spectrum. Figures 2(a) and 2(b) show doping-dependent color maps of the PL spectra in ML and BL WSe_2, respectively, with 100 μW excitation power. In the ML, as electrons are removed from the sample by applying a negative gate voltage, the PL intensity of X^0 increases as the sample becomes more charge neutral, whereas the PL intensity of XX^- rapidly decreases [see Fig. 2(a)]. The XX^- peak exists only between the crossover from neutral to the n-doped regime, implying that it is indeed negatively charged (formed from a bound state of X^- and X^D). Electron doping through electrostatic back-gate voltage (V_g; $0\,\mathrm{V} < V_g < 30\,\mathrm{V}$) leads to conversion of X^0 to X^-. Enhancement of the XX^- peak upon further electron doping ($V_g < 60$ V) is observed, which is possibly due to emergence of X^{--} [27,31]. Figure 2(c) shows integrated intensity of different peaks in the ML as a function of the gate voltage.

For the BL [Fig. 2(b)], with application of high negative gate voltages, a peak emerges that is attributed to X^+ [also indicated in Fig. 2(a)]. Figure 2(d) shows the PL intensity as a function of gate voltage in BL WSe_2. Here, X^0, X^-, and XX^- show a doping dependence like in the ML. From the color plot of Fig. 2(b), we also observe a broad low-energy indirect exciton X^I peak ≈ 1.55 eV. Specific domes of high PL intensity of X^I peaks of BL WSe_2 emerge as electrostatic doping is modified, which could possibly be related to resonant exciton-phonon scattering [39]. The domes of high PL have not been studied in a second device but are hinted by previous work [23,40]. A systematic experimental and theoretical study is

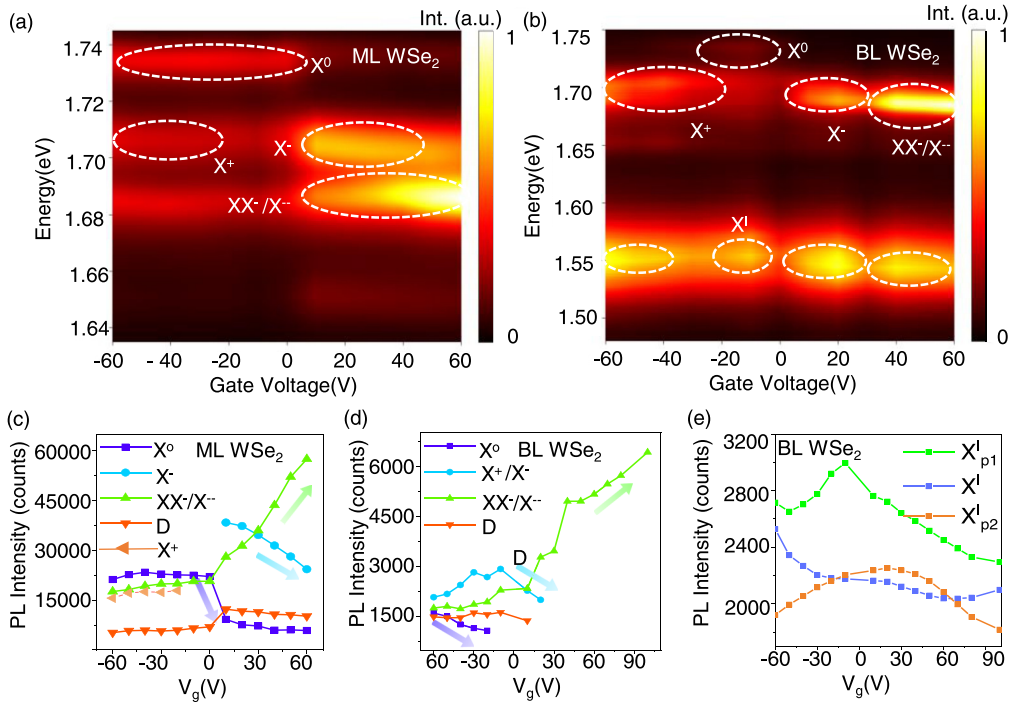

FIG. 2. Photoluminescence (PL) spectra of monolayer (ML) and bilayer (BL) WSe_2 under charge doping. (a) and (b) Color plot of PL spectra as a function of gate voltage in the BL and ML. Regions of existence of different excitonic states under charge doping are indicated by dotted curves. (c) and (d) PL intensity of different excitonic complexes as a function of gate voltage in the ML and BL, respectively. (e) PL intensities of the interlayer (IL) excitons and phonon replicas as a function of gate voltage in the BL.

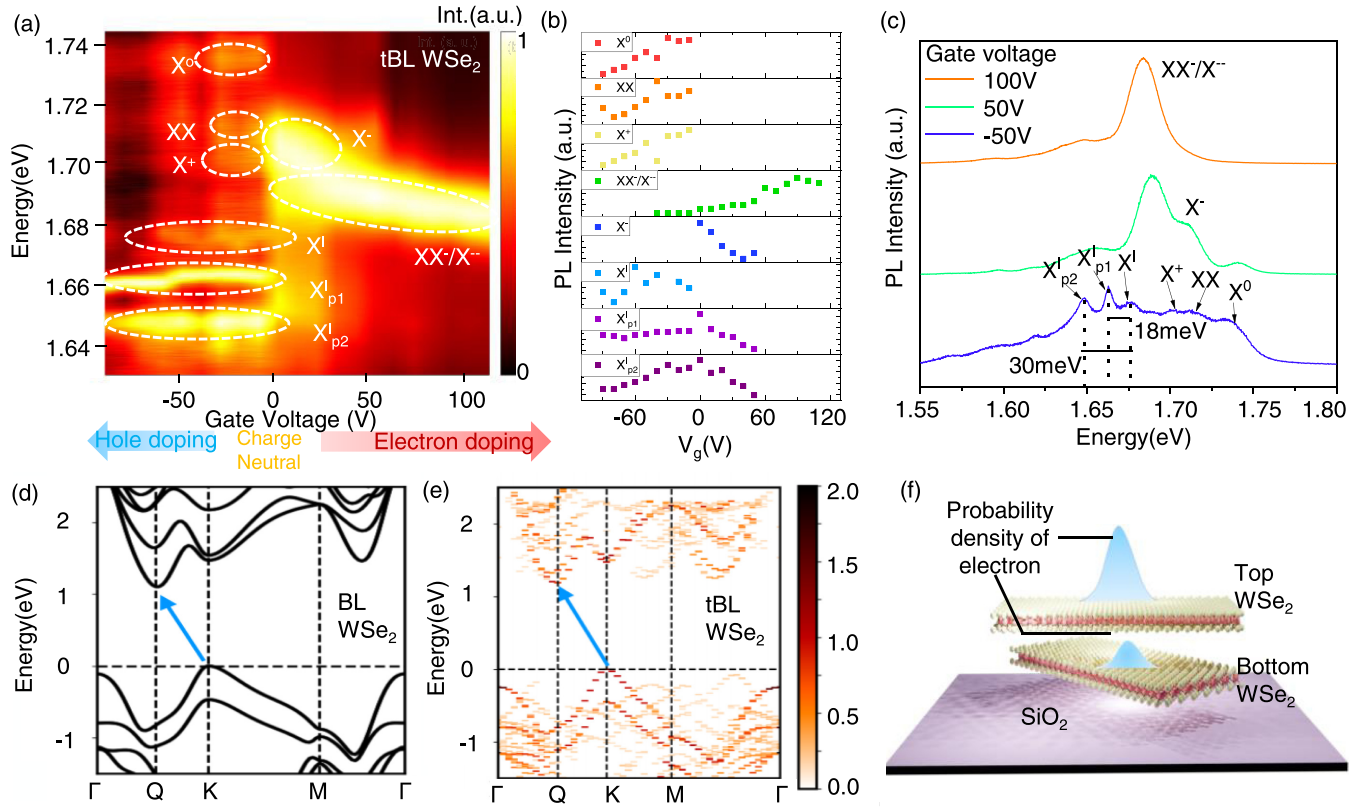

FIG. 3. Electrical tuning of excitonic states in twisted bilayer (tBL) WSe_2. (a) Color map of photoluminescence (PL) spectra as a function of gate voltage in tBL WSe_2. Regions of existence of different excitonic states under charge doping are indicated by dotted curves. (b) PL intensity of different excitonic species as a function of gate voltage. (c) PL spectra at 7 K at different doping densities (gate voltages). (d) The calculated band structure of bilayer (BL) WSe_2 and (e) unfolded band structure of 21° commensurate tBL WSe_2. The arrows show the indirect energy bandgap. Note: Valence band maximum is set to zero. (f) Schematic of electron probability density distribution in tBL WSe_2.

required to understand its origin and behavior with doping. More details are discussed in the Supplemental Material [33].

Figure 3(a) shows the doping-dependent energy mapping of tBL WSe_2. Figure 3(b) shows the peak intensity of different excitonic peaks in the tBL as a function of doping. Multipeak Lorentzian fits to the PL spectra for all devices at *p*- and *n*-doping conditions are given in Supplemental Material Sec. II [33]. Like the case of the ML and BL, XX^- (X^{--}) shows an increase in intensity with electron doping, the trion intensity decreases, while the neutral exciton vanishes. PL peak positions as a function of back-gate voltage are discussed in Supplemental Material Sec. III [33].

Interestingly, we observe a distinct peak ∼1.71 eV, which lies 20 meV below X^0. This coincides with energy spacing of XX in the hexagonal boron nitride-encapsulated ML and is thus attributed similarly, with supporting arguments below [20,29–31]. Unlike X^- and XX^-, which extends to the *n*- or *p*-doped region, the XX peak is restricted to the intrinsic region only. The BEs (Δ) of the neutral and charged biexciton are given as $\Delta_{XX} = \hbar\omega_{X^0} - \hbar\omega_{XX}$ and $\Delta_{XX^-} = \hbar\omega_{X^-} - \hbar\omega_{XX^-}$, respectively [25]. Here, we consider that the emission is due to the dissociation of XX^- into X^D and X^-, and XX into X^D and X^0. A schematic of the process is given in Supplemental Material Sec. IV [33]. Thus, the BEs of XX^- and XX need to be counted from the X^- and X^0 emission energy, respectively. BEs measured thus are 19 meV for XX and 17 meV for XX^-, in good agreement with theoretical predictions [41]. The energetic peak position and the doping dependence suggest that the peak at 1.71 eV is indeed the neutral biexciton peak. We have calculated similar BE from thermal activation studies (last section), thus providing further evidence for the peak assignment. We also studied the dependence of laser power on PL spectra. The XX peak intensity shows a super-linear dependence on laser power, with the power exponent (α) 1.25, while X has a power coefficient of 1. Details have been discussed in Supplemental Material Sec. IV [33].

Interestingly, XX is not visible in nonencapsulated ML or BL WSe_2, and its observation in the nonencapsulated tBL indicates the uniqueness of the intermediate misorientation tBL regarding coupling and screening. Owing to the small IL coupling (see Supplemental Material Sec. V [33] for details) at large angles, the two layers of WSe_2 behave as a moderately decoupled system, resulting in a partial screening of the top layer from the disorder-inducing potential fluctuations of the bottom SiO_2. This may lead to sharper spectral transitions in the tBL (where we observe the neutral XX and well-separated indirect excitons) with less broadening in the peak width than the ML and BL, with the additional knob of valley band alignment.

D. Indirect exciton and phonon replica

We now focus on the low-energy (1.5–1.65 eV) peaks in tBL WSe_2, corresponding to the momentum-indirect excitons (X^I). They are dependent on the IL coupling, which is significant even at the intermediate twist angle of 20° [37,40]. Figure 3(a) shows the energy mapping of the indirect excitons of tBL WSe_2. We note that the indirect peak of tBL WSe_2 is blueshifted by 105 meV as compared with the BL. We performed DFT calculations, as solving the Bethe-Salpeter equation for a tBL is computationally prohibitive. As the polarizability is similar in the tBL and BL, we analyze the excitons qualitatively with the input from the electronic structure calculations. Since the relaxation effect is small and the moiré potential is weak in this system, the wave functions at the band edges do not localize at a particular stacking. The shift in the exciton spectra can therefore be related to the modification of the band structure induced by a twist in 21° commensurate tBL WSe_2. At a large twist angle, the hybridization of the individual layers quenches significantly, resulting in reduction of the IL coupling, which modifies the Q valley of the Brillouin zone. Unfolding the band structure of the 21° tBL to the unit cell Brillouin zone shows that the conduction band minimum has shifted from the Q point to a nearby point. We call this point Q', which is not along the Γ-K direction in the unit cell Brillouin zone (see Supplemental Material [33]). The blueshift of the indirect exciton can be compared with the shift of the Q valley in the calculated electronic band structure. The lowest indirect transition energy of the tBL increases by 78 meV compared with that of the BL [Figs. 3(d) and 3(e)]. This compares well with the experimentally observed blueshift of the indirect peak.

Figures 3(a) and 3(c) show two more sharp peaks with redshifted energies of 18 and 30 meV from the X^I emission peak. These peaks have recently been observed as two-phonon replicas (X^I_{p1}, X^I_{p2} of exciton), where nearly resonant exciton-phonon scattering processes take place [38,39]. In the BL, the shifts are 20 and 41 meV. Additionally, we find that the phonon replicas are much brighter than their primary emission peak. In the tBL, these peaks are also much sharper, suggesting a layer-dependent asymmetric electron probability density, which depends upon the twist angle of a tBL [36,42,43] [see Fig. 3(f)]. More details about this are given in Supplemental Material Sec. III [33].

Remarkably, the indirect excitonic states of tBL WSe_2 show an asymmetric dependence on doping density [see Fig. 3(c)]. With increasing electron carrier density, indirect excitons strongly quench in the tBL [also see Fig. 3(a)]. On the other hand, indirect excitons in the BL show an oscillatory intensity profile on both the electron- and hole-doped side. This distinct gate dependence can be understood qualitatively by the Q' valley population of tBL and BL WSe_2. The spectral emission depends on both the oscillator strength and the electron population density. The band structure of tBL WSe_2 in the moiré Brillouin zone is given in Supplemental Material Sec. V [33]. For the tBL, the energy difference (Δ) between the conduction band minimum at Q' (Q for the BL) and the conduction band edge at the K valley is 295 meV, whereas in the BL, it is 366 meV [see Figs. 3(d) and 3(e)]. Further, tuning the gate voltage in the n-doped regime leads to an upward shift of the quasi-Fermi level of the system (see Fig. S13 in the Supplemental Material [33] for details), resulting in an effective density tuning of both the Q and K valleys, as well as phase filling of primarily the Q valley. When the energy difference of the conduction band edges at the Q and K valleys reduces, the probability of photo-excited electrons relaxing to the K valley and subsequent direct radiative transitions will be enhanced. Since momentum-direct K-K transitions are more probable than momentum-indirect Q'-K transitions, negatively charged trions and biexcitons increase with n doping, and indirect excitons quickly vanish. In contrast, for the case of the BL, the energy difference between the Q and K valleys is much higher, and thus, even in the high n-doped regime, photo-excited electrons are mostly localized at the Q valley, leading to indirect exciton PL emission. The other two peaks (X^I_{p1}, X^I_{p2}) have similar doping dependence as X^I and are thus again attributed to two-phonon replicas of X^I [38].

E. Thermal disassociation of many-body charge

To further clarify the underlying exciton interactions, we perform thermal activation measurements. Figures 4(a) and 4(b) show the temperature dependence of ML and tBL WSe_2 at the p-doped region ($Vg = -60$ V), and similarly, Figs. 4(c) and 4(d) correspond to the n-doped region ($Vg = 60$ V). Similar color plots for the BL are given in Supplemental Material Sec. IV [33]. In the p-doped regime, the high-temperature PL spectrum of ML WSe_2 is mainly dominated by X^0 due to its large BE of ≈400 meV. The n-doped regions for the ML and tBL are solely dominated by XX^- (or X^{--}), which survives up to 80 K, implying the thermal robustness of the charged complex. In the near charge-neutral region in tBL WSe_2, XX is found to survive to much higher temperatures. At low temperatures, the optical response shifts toward the indirect PL peaks (at p doping), along with two-phonon replica peaks. The indirect peaks are highly sensitive to temperature because the exciton distribution becomes very narrow in momentum space at low temperature.

In Figs. 5(a) and 5(b), we plot the PL spectra of ML and tBL WSe_2 in the near charge-neutral region at different temperatures. As the temperature increases, we observe that the overall emission intensities gradually increase and then surprisingly decrease beyond 112 K. Nonradiative recombination is a dominant process at high temperatures and leads to thermal quenching. For example, the PL intensity of MoS_2 decreases monotonically with increasing temperature [44]. For WSe_2, on the other hand, the PL intensity generally increases with temperature due to quenching of dark excitons and enhancement of the population of bright excitons [45]. Here, we observe negative thermal quenching in the tBL, which can be understood as the thermal activation to the exciton and trion states from the low-energy states, resulting in an increase in the population of the higher-energy excitonic complexes [46].

Analysis of the thermally activated behavior provides insight into the BEs and the formation and dissociation dynamics of the excitonic complexes XX and XX^-. If we consider the high density of dark excitons at low temperatures [45], then the formation process of excitonic complexes is limited by the population of minority species, i.e., formation of XX is limited by population of X^0, and XX^- by X^- [20]. To quantitatively understand the thermal dissociation process,

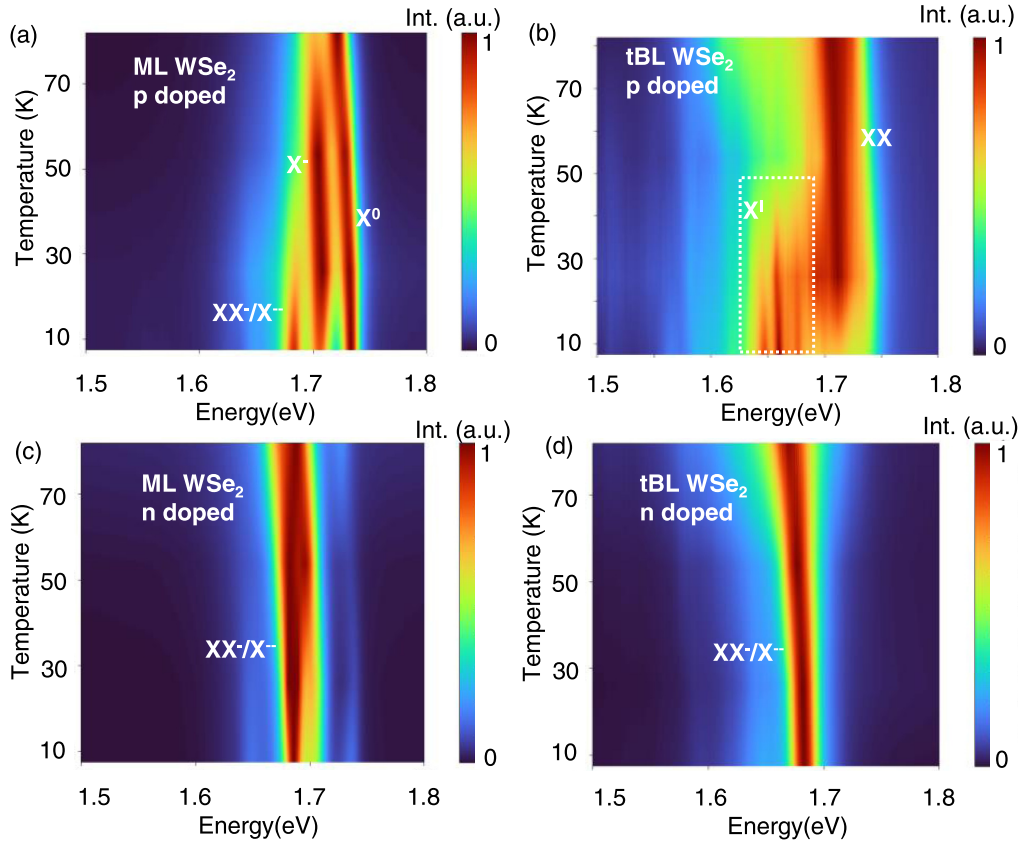

FIG. 4. Thermally activated photoluminescence (PL) spectra of monolayer (ML) and twisted bilayer (tBL) WSe_2. (a) and (b) Color plot of PL spectra as a function of temperature in the ML and tBL, respectively, at $V_g = -60$ V in the hole-doped regime. (c) and (d) Color plot of PL spectra as a function of temperature in the ML and tBL, respectively, at $V_g = 60$ V in the electron-doped regime.

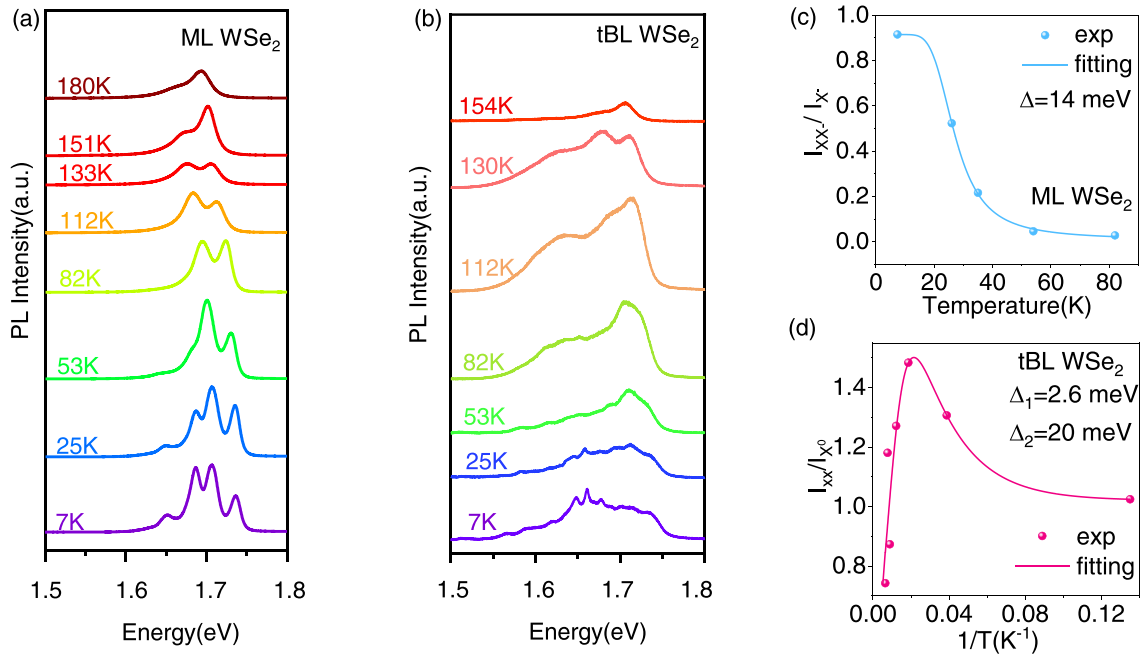

FIG. 5. Temperature dependence of spectral emissions in monolayer (ML) and twisted bilayer (tBL) WSe_2. (a) and (b) Photoluminescence (PL) spectra at different temperatures in the ML and tBL, respectively. PL spectra in (a) and (b) have been vertically shifted for clarity. The spectra have not been normalized to aid visualization of temperature dependence of the PL intensity. (c) Normalized excitonic intensity of XX^- to X^- in the ML as a function of temperature. The solid line is the fit to Eq. (1). (d) Normalized excitonic intensity of XX to X^0 in the tBL as a function of temperature. The solid line is the fit to Eq. (2).

we normalize the intensity of XX^- to the intensity of X^- in the case of ML WSe_2 [see Fig. 5(c)], and the intensity of XX to the intensity of X^0 in the case of tBL WSe_2 [see Fig. 5(d)] [25]. We observe normal thermal quenching for XX^- in the ML, and this thermally activated disassociation can be captured by using the thermal activation equation considering only one BE Δ [19,46]:

$$I(T) = \frac{I(0)}{1 + A\exp\left(-\frac{\Delta}{k_B T}\right)}, \tag{1}$$

where $I(0)$ is the intensity at 0 K, Δ is the BE, k_B is the Boltzmann constant, and A is a fitting parameter. Using Eq. (1) to fit our experimental data, we find that Δ of XX^- is 14 $\pm$ 3 meV. In this paper, we have followed a previously used framework (Ref. [25]) to estimate the BEs of biexcitons. This method gives us a rough estimate of the BE since the entropy of ionization is not included (Refs. [47,48]).

To understand negative thermal quenching in tBL WSe_2, the multilevel model for the temperature dependence of the PL peak intensities is given by [46,49]

$$I(T) = I(0)\frac{1 + A\exp\left(-\frac{\Delta_1}{k_B T}\right)}{1 + B\exp\left(-\frac{\Delta_2}{k_B T}\right)}, \tag{2}$$

where A and B are fitting parameters. Here, Δ_1 describes the thermal activation energy corresponding to the increment of the PL intensity with temperature, whereas Δ_2 represents the activation energy for the thermal quenching process. For a two-level system, the BE of XX is given by $\Delta_2 - \Delta_1 = 17 \pm 5$ meV. The BE values for both XX and XX^- are in reasonable agreement with earlier calculations $\Delta_{XX} = 20.7$ meV and $\Delta_{XX^-} = 14.9$ meV [41].

III. CONCLUSIONS

In summary, we have observed many-body correlated excitonic states in ML, BL, and tBL WSe_2. Low-temperature PL reveals several higher-order excitonic states, including the neutral biexciton, which was observed only in tBL WSe_2, showing the versatility of the tBL in providing an interesting testbed for light-matter interactions. In the tBL, XX is dominant in the p-doped regime at high temperatures, while XX^- is dominant in the n-doped regime. The stability of these higher-order excitonic complexes at high temperatures makes the tBL an exciting prototype for exploring multibody correlated physics even at high temperatures. Remarkably, the indirect excitons in the tBL vanish in the electron-doped regime due to the twist-angle-related modification of the band structure. Through DFT calculations, we find that Q'-K band alignment is related to vanishing of indirect excitons in the electron-doped regime as well as blueshift of indirect excitons in the tBL (compared with the BL). In general, in this paper, we provide an improved physical understanding of the complex excitonic states through the interplay of charge, temperature, and twist angle. The studies can be extended to manipulation of excitons for applications such as exciton lasing by coupling to a photonic cavity and for harvesting high-order excitonic states for potential applications in sensing, imaging, nanophotonics, and valleytronics.

IV. MATERIALS AND METHODS

A. Experiment

1. PL spectroscopy

PL spectra of WSe_2 flakes were taken using a Horiba LabRAM HR spectrometer. We performed the measurements at the same experimental parameters for all samples to remove any ambiguity. We used a 532 nm laser with laser power 72 μW, a 50× long working distance objective with NA 0.5, an integration time of 30 s, and a laser spot size ∼0.5 μm. A low-temperature Montana cryostat was used to measure PL spectra at low temperatures.

2. SHG measurements

Polarization-dependent SHG measurements were performed using a nonlinear microscopy imaging setup with a linearly polarized femtosecond laser (Fidelity HP-10 laser, 80 MHz repetition rate, wavelength at 1040 nm, and pulse duration of 140 fs) used as an excitation source. The input laser is focused using a 20 × /0.75 NA objective lens, and the same objective is used to collect the backward SHG signal. The SHG signal is detected using a photomultiplier tube with a dichroic filter, a set of bandpass (520/15 nm) and short pass (890 nm) filters, and a polarizer (analyzer) mounted in front of it for rejecting the fundamental source and minimizing the background noise. For the twist angle measurement, the sample is rotated from 0–90° in steps of 5° with respect to the laboratory horizontal axis, keeping the input polarizer and the output analyzer fixed and in parallel with the laboratory horizontal axis. For each angle, SHG images of the twisted sample are acquired and later analyzed to calculate the twist angle.

3. DFT calculations

The QUANTUM ESPRESSO package [50] was used to perform the DFT calculations of BL and tBL WSe_2. The exchange correlation was approximated with the local gradient approximation [51]. The unit cell Brillouin zone was sampled with 12 × 12 Monkhorst-Pack k-grid [52], and the moiré Brillouin zone was scaled accordingly. The band structure of the 21° commensurate tBL WSe_2 was calculated in the moiré Brillouin zone and unfolded to the unit cell Brillouin zone [53] to identify the band edges.

ACKNOWLEDGMENTS

The authors acknowledge financial support from U.S. Army International Technology Center Pacific and the Ministry of Electronics and Information Technology, Government of India, as well as the Supercomputer Education and Research Centre at IISc for providing computational resources. A.S. acknowledges funding from an IISc startup grant.

R.D. and S.S. contributed equally to this paper.

The authors declare no competing financial interests.

[1] H. Yu, G.-B. Liu, J. Tang, X. Xu, and W. Yao, Sci. Adv. **3**, e1701696 (2017).

[2] K. Tran, J. Choi, and A. Singh, 2D Mater. **8**, 022002 (2021).

[3] T. I. Andersen, G. Scuri, A. Sushko, K. De Greve, J. Sung, Y. Zhou, D. S. Wild, R. J. Gelly, H. Heo, D. Bérubé *et al.*, Nat. Mater. **20**, 480 (2021).

[4] S. Brem, K.-Q. Lin, R. Gillen, J. M. Bauer, J. Maultzsch, J. M. Lupton, and E. Malic, Nanoscale **12**, 11088 (2020).

[5] K. Tran, G. Moody, F. Wu, X. Lu, J. Choi, K. Kim, A. Rai, D. A. Sanchez, J. Quan, A. Singh *et al.*, Nature (London) **567**, 71 (2019).

[6] C. Jin, E. C. Regan, A. Yan, M. I. B. Utama, D. Wang, S. Zhao, Y. Qin, S. Yang, Z. Zheng, S. Shi *et al.*, Nature (London) **567**, 76 (2019).

[7] S. Brem, C. Linderälv, P. Erhart, and E. Malic, Nano Lett. **20**, 8534 (2020).

[8] E. M. Alexeev, D. A. Ruiz-Tijerina, M. Danovich, M. J. Hamer, D. J. Terry, P. K. Nayak, S. Ahn, S. Pak, J. Lee, J. I. Sohn *et al.*, Nature (London) **567**, 81 (2019).

[9] H. Baek, M. Brotons-Gisbert, Z. Koong, A. Campbell, M. Rambach, K. Watanabe, T. Taniguchi, and B. D. Gerardot, Sci. Adv. **6**, eaba8526 (2020).

[10] M. Brotons-Gisbert, H. Baek, A. Campbell, K. Watanabe, T. Taniguchi, and B. D. Gerardot, Phys. Rev. X **11**, 031033 (2021).

[11] Y. Tang, J. Gu, S. Liu, K. Watanabe, T. Taniguchi, J. Hone, K. F. Mak, and J. Shan, Nat. Nanotechnol. **16**, 52 (2021).

[12] E. C. Regan, D. Wang, C. Jin, M. I. B. Utama, B. Gao, X. Wei, S. Zhao, W. Zhao, Z. Zhang, K. Yumigeta *et al.*, Nature (London) **579**, 359 (2020).

[13] C. Jin, Z. Tao, T. Li, Y. Xu, Y. Tang, J. Zhu, S. Liu, K. Watanabe, T. Taniguchi, J. C. Hone *et al.*, Nat. Mater. **20**, 940 (2020).

[14] Y. You, X.-X. Zhang, T. C. Berkelbach, M. S. Hybertsen, D. R. Reichman, and T. F. Heinz, Nat. Phys. **11**, 477 (2015).

[15] M. He, P. Rivera, D. Van Tuan, N. P. Wilson, M. Yang, T. Taniguchi, K. Watanabe, J. Yan, D. G. Mandrus, H. Yu *et al.*, Nat. Commun. **11**, 618 (2020).

[16] S. Latini, K. T. Winther, T. Olsen, and K. S. Thygesen, Nano Lett. **17**, 938 (2017).

[17] S. Huang, X. Ling, L. Liang, J. Kong, H. Terrones, V. Meunier, and M. S. Dresselhaus, Nano Lett. **14**, 5500 (2014).

[18] K. Liu, L. Zhang, T. Cao, C. Jin, D. Qiu, Q. Zhou, A. Zettl, P. Yang, S. G. Louie, and F. Wang, Nat. Commun. **5**, 4966 (2014).

[19] J. S. Ross, S. Wu, H. Yu, N. J. Ghimire, A. M. Jones, G. Aivazian, J. Yan, D. G. Mandrus, D. Xiao, W. Yao *et al.*, Nat. Commun. **4**, 1474 (2013).

[20] Z. Li, T. Wang, Z. Lu, C. Jin, Y. Chen, Y. Meng, Z. Lian, T. Taniguchi, K. Watanabe, S. Zhang *et al.*, Nat. Commun. **9**, 3719 (2018).

[21] K. He, N. Kumar, L. Zhao, Z. Wang, K. F. Mak, H. Zhao, and J. Shan, Phys. Rev. Lett. **113**, 026803 (2014).

[22] G. Wang, X. Marie, L. Bouet, M. Vidal, A. Balocchi, T. Amand, D. Lagarde, and B. Urbaszek, Appl. Phys. Lett. **105**, 182105 (2014).

[23] J. Lindlau, M. Selig, A. Neumann, L. Colombier, J. Förste, V. Funk, M. Förg, J. Kim, G. Berghäuser, T. Taniguchi *et al.*, Nat. Commun. **9**, 2586 (2018).

[24] D. K. Zhang, D. W. Kidd, and K. Varga, Nano Lett. **15**, 7002 (2015).

[25] S.-Y. Chen, T. Goldstein, T. Taniguchi, K. Watanabe, and J. Yan, Nat. Commun. **9**, 3717 (2018).

[26] E. Liu, J. van Baren, T. Taniguchi, K. Watanabe, Y.-C. Chang, and C. H. Lui, Phys. Rev. Research **1**, 032007(R) (2019).

[27] Z. Li, T. Wang, C. Jin, Z. Lu, Z. Lian, Y. Meng, M. Blei, S. Gao, T. Taniguchi, K. Watanabe *et al.*, Nat. Commun. **10**, 2469 (2019).

[28] J. Förste, N. V. Tepliakov, S. Y. Kruchinin, J. Lindlau, V. Funk, M. Förg, K. Watanabe, T. Taniguchi, A. S. Baimuratov, and A. Högele, Nat. Commun. **11**, 4539 (2020).

[29] A. Steinhoff, M. Florian, A. Singh, K. Tran, M. Kolarczik, S. Helmrich, A. W. Achtstein, U. Woggon, N. Owschimikow, F. Jahnke *et al.*, Nat. Phys. **14**, 1199 (2018).

[30] K. Hao, J. F. Specht, P. Nagler, L. Xu, K. Tran, A. Singh, C. K. Dass, C. Schüller, T. Korn, M. Richter *et al.*, Nat. Commun. **8**, 15552 (2017).

[31] M. Barbone, A. R.-P. Montblanch, D. M. Kara, C. Palacios-Berraquero, A. R. Cadore, D. De Fazio, B. Pingault, E. Mostaani, H. Li, B. Chen *et al.*, Nat. Commun. **9**, 3721 (2018).

[32] R. Debnath, S. Sett, R. Biswas, V. Raghunathan, and A. Ghosh, Nanotechnology **32**, 455705 (2021).

[33] See Supplemental Material at http://link.aps.org/supplemental/10.1103/PhysRevB.106.125409 for details of device fabrication and twist angle characterization through SHG, details of the multipeak fittings, determination of the binding energy, power dependence of the excitonic peaks, details of the band structure of the twisted WSe_2, temperature dependence PL spectra, details of the asymmetry in the indirect excitonic peak and Fermi level shift with doping in twisted WSe_2.

[34] E. Courtade, M. Semina, M. Manca, M. M. Glazov, C. Robert, F. Cadiz, G. Wang, T. Taniguchi, K. Watanabe, M. Pierre *et al.*, Phys. Rev. B **96**, 085302 (2017).

[35] Z. Li, T. Wang, C. Jin, Z. Lu, Z. Lian, Y. Meng, M. Blei, M. Gao, T. Taniguchi, K. Watanabe *et al.*, ACS Nano **13**, 14107 (2019).

[36] P. Merkl, F. Mooshammer, S. Brem, A. Girnghuber, K.-Q. Lin, L. Weigl, M. Liebich, C.-K. Yong, R. Gillen, J. Maultzsch *et al.*, Nat. Commun. **11**, 2167 (2020).

[37] Z. Wang, Y.-H. Chiu, K. Honz, K. F. Mak, and J. Shan, Nano Lett. **18**, 137 (2018).

[38] M. M. Altaiary, E. Liu, C.-T. Liang, F.-C. Hsiao, J. van Baren, T. Taniguchi, K. Watanabe, N. M. Gabor, Y.-C. Chang, and C. H. Lui, arXiv:2101.11161.

[39] M. M. Altaiary, E. Liu, C.-T. Liang, F.-C. Hsiao, J. van Baren, T. Taniguchi, K. Watanabe, N. M. Gabor, Y.-C. Chang, and C. H. Lui, Nano Lett. **22**, 1829 (2022).

[40] G. Scuri, T. I. Andersen, Y. Zhou, D. S. Wild, J. Sung, R. J. Gelly, D. Bérubé, H. Heo, L. Shao, A. Y. Joe *et al.*, Phys. Rev. Lett. **124**, 217403 (2020).

[41] I. Kylänpää and H.-P. Komsa, Phys. Rev. B **92**, 205418 (2015).

[42] J. Sung, Y. Zhou, G. Scuri, V. Zólyomi, T. I. Andersen, H. Yoo, D. S. Wild, A. Y. Joe, R. J. Gelly, H. Heo *et al.*, Nat. Nanotechnol. **15**, 750 (2020).

[43] A. Weston, Y. Zou, V. Enaldiev, A. Summerfield, N. Clark, V. Zólyomi, A. Graham, C. Yelgel, S. Magorrian, M. Zhou *et al.*, Nat. Nanotechnol. **15**, 592 (2020).

[44] J. Pei, J. Yang, R. Xu, Y.-H. Zeng, Y. W. Myint, S. Zhang, J.-C. Zheng, Q. Qin, X. Wang, W. Jiang *et al.*, Small **11**, 6384 (2015).

[45] S. Brem, A. Ekman, D. Christiansen, F. Katsch, M. Selig, C. Robert, X. Marie, B. Urbaszek, A. Knorr, and E. Malic, Nano Lett. **20**, 2849 (2020).

[46] H. Shibata, Jpn. J. Appl. Phys. **37**, 550 (1998).

[47] R. A. Kaindl, D. Hägele, M. A. Carnahan, and D. S. Chemla, Phys. Rev. B **79**, 045320 (2009).
[48] J. Mock, G. Thomas, and M. Combescot, Solid State Commun. **25**, 279 (1978).
[49] J. Huang, T. B. Hoang, and M. H. Mikkelsen, Sci. Rep. **6**, 22414 (2016).
[50] P. Giannozzi, S. Baroni, N. Bonini, M. Calandra, R. Car, C. Cavazzoni, D. Ceresoli, G. L. Chiarotti, M. Cococcioni, I. Dabo *et al.*, J. Phys.: Condens. Matter **21**, 395502 (2009).
[51] J. P. Perdew and A. Zunger, Phys. Rev. B **23**, 5048 (1981).
[52] H. J. Monkhorst and J. D. Pack, Phys. Rev. B **13**, 5188 (1976).
[53] V. Popescu and A. Zunger, Phys. Rev. B **85**, 085201 (2012).